Title: **Mechanistic understanding enables the rational design of salicylanilide combination therapies for Gram-negative infections**

Running title: Countering salicylanilide resistance in Gram negatives

Authors: Janine N. Copp[#,1,2], Daniel Pletzer[3]* , Alistair S. Brown[1], Joris Van der Heijden[2]*, Charlotte M. Miton[2], Rebecca J. Edgar[1], Michelle H. Rich[1]*, Rory F Little[1], Elsie M. Williams[1], Robert E.W. Hancock[3], Nobuhiko Tokuriki[2], David F. Ackerley[#,1,4]

[1]School of Biological Sciences, Victoria University of Wellington, Wellington, New Zealand. [2]Michael Smith Laboratories, University of British Columbia, Vancouver, Canada. [3]Center for Microbial Diseases and Immunity Research, Department of Microbiology and Immunology, University of British Columbia, Vancouver, Canada. [4]Centre for Biodiscovery, Victoria University of Wellington, Wellington, New Zealand.

[#]Correspondence: janine.copp@msl.ubc.ca; david.ackerley@vuw.ac.nz

*Present addresses: Daniel Pletzer, Department of Microbiology and Immunology, University of Otago, New Zealand; Joris Van der Heijden, Ottawa Virus Manufacturing Facility, Ottawa Hospital Research Institute, Ottawa, Canada; Michelle Rich, School of Biomolecular and Biomedical Sciences, O'Brien Centre for Science, University College Dublin, Ireland

Keywords: Synergy, repurposing, niclosamide, colistin, efflux, nitroreductase, resistance, proton motive force

Abstract

One avenue to combat multidrug-resistant Gram-negative bacteria is the co-administration of multiple drugs (combination therapy), which can be particularly promising if drugs synergize. The identification of synergistic drug combinations, however, is challenging. Detailed understanding of antibiotic mechanisms can address this issue by facilitating the rational design of improved combination therapies. Here, using diverse biochemical and genetic assays, we reveal the molecular mechanisms of niclosamide, a clinically-approved salicylanilide compound, and demonstrate its potential for Gram-negative combination therapies. We discovered that Gram-negative bacteria possess two innate resistance mechanisms that reduce their niclosamide susceptibility: a primary mechanism mediated by multidrug efflux pumps and a secondary mechanism of nitroreduction. When efflux was compromised, niclosamide became a potent antibiotic, dissipating the proton motive force (PMF), increasing oxidative stress and reducing ATP production to cause cell death. These insights guided the identification of diverse compounds that synergized with salicylanilides when co-administered (efflux inhibitors, membrane permeabilizers, and antibiotics that are expelled by PMF-dependent efflux), thus suggesting that salicylanilide compounds may have broad utility in combination therapies. We validate these findings *in vivo* using a murine abscess model, where we show that niclosamide synergizes with the membrane permeabilizing antibiotic colistin against high-density infections of multidrug-resistant Gram-negative clinical isolates. We further demonstrate that enhanced nitroreductase activity is a potential route to adaptive niclosamide resistance but show that this causes collateral susceptibility to clinical nitro-prodrug antibiotics. Thus, we highlight how mechanistic understanding of mode of action, innate/adaptive resistance, and synergy can rationally guide the discovery, development and stewardship of novel combination therapies.

Importance

There is a critical need for more effective treatments to combat multidrug-resistant Gram-negative infections. Combination therapies are a promising strategy, especially when these

enable existing clinical drugs to be repurposed as antibiotics. We reveal the mechanisms of action and basis of innate Gram-negative resistance for the anthelmintic drug niclosamide, and subsequently exploit this information to demonstrate that niclosamide and analogs kill Gram-negative bacteria when combined with antibiotics that inhibit drug efflux or permeabilize membranes. We confirm the synergistic potential of niclosamide *in vitro* against a diverse range of recalcitrant Gram-negative clinical isolates, and *in vivo* in a mouse abscess model. We also demonstrate that nitroreductases can confer resistance to niclosamide, but show that evolution of these enzymes for enhanced niclosamide resistance confers a collateral sensitivity to other clinical antibiotics. Our results highlight how detailed mechanistic understanding can accelerate the evaluation and implementation of new combination therapies.

Introduction

New therapeutic strategies are urgently required to combat multidrug-resistant (MDR) Gram-negative bacteria (1). The co-administration of two or more drugs (combination therapy) (2) is a promising approach, especially if the drugs exhibit synergy, *i.e.*, enhanced efficacy over the predicted additive effects (3, 4). Synergistic combination therapies can kill microbes that are resistant to one of the drugs in the pair, may slow the evolution of resistance (5-7), and can facilitate the use of lower doses of each drug, thus reducing side effects and adverse reactions (8). The identification of synergistic drug combinations, however, is challenging due to the infrequency of synergistic relationships and the substantial scale of combinatorial drug screening (*e.g.*, for a collection of 1,000 compounds, 499,500 pairwise combinations are possible, even before considering optimal relative concentrations) (3, 4). Mechanistic understanding of synergy may reveal novel antibiotic targets and guide the rational design of superior drug combinations *e.g.*, the co-administration of β-lactam compounds and β-lactamase inhibitors (9). However, for the majority of combination therapies the underlying basis of synergism is unclear. Indeed, despite clinical use for almost 50 years, the synergism of trimethoprim and sulfamethoxazole was only explored in detail in 2018 (10). Combination therapy may also enable compounds that have been clinically approved for other conditions, *e.g.*,

antidepressants, antipsychotics, and antidiarrhetics (11-13), to be repurposed as antibiotics; such compounds typically have detailed data regarding their toxicity, formulation and pharmacology that can expedite their clinical progression (14). However, the screening of clinical compounds for repurposing potential is laborious and often necessitates high throughput robotic systems (13, 15). Detailed knowledge of the antibiotic mechanisms of action of promising clinical compounds would accelerate drug repurposing approaches and enable the circumvention of resistance mechanisms that may mask activity in initial screens. Thus, comprehensive understanding of both the mode of action and innate resistance mechanisms is important to inform the rational design of superior combination therapies that harness repurposed clinical compounds.

Niclosamide (**Fig. 1a**) is a clinically-approved drug that has been used to treat helminth parasites in humans and animals for more than 50 years (16). Recently, several studies have suggested the potential of repurposing niclosamide for other medical applications, *e.g.*, niclosamide appears to modulate metabolic disorders and neurological conditions, and has antiproliferative effects against various cancers (17). The diverse pharmacological activities of niclosamide are likely the result of oxidative phosphorylation uncoupling and the modulation of signaling pathways (18, 19). Niclosamide exhibits antiviral activity against SARS-COV (20, 21), and is an effective antibiotic against Gram-positive and acid-fast pathogens (*e.g. Staphylococcus aureus and Mycobacterium tuberculosis*), as well as *Helicobacter pylori* (22-24). As an anti-infective, the low absorption and poor oral bioavailability of niclosamide may hamper its use (25), however optimized derivatives, nano-based formulations and/or local administration may rescue its therapeutic potential (26-28). In isolation, niclosamide exhibits no activity against most Gram-negative pathogens (1, 23). Nevertheless, it was recently reported that *in vitro* co-administration of niclosamide and colistin can overcome colistin-resistance in Gram-negative bacteria (29-31). While these findings suggest that niclosamide may hold cryptic antibiotic potential, the molecular basis that underlies its antibiotic mode of action, synergy, and the lack of efficacy against Gram-negative bacteria has been hitherto unknown.

In this work, we uncover the innate resistance mechanisms and antibacterial mode of action of niclosamide and related salicylanilide analogs, thus revealing their therapeutic potential

as potent antibiotics when utilized in rationally designed combination therapies**.** We reveal a potential route to adaptive niclosamide resistance, but demonstrate that this leads to collateral susceptibility; thus, the emergence of resistance via this route may be prevented or slowed in the clinic. In addition, we demonstrate the *in vitro* efficacy of niclosamide combination therapy against MDR Gram-negative clinical isolates, and confirm synergy *in vivo* using in a murine abscess model using high density infections that mimics a clinical situation where antibiotics typically fail (32).

Results

TolC-mediated efflux and nitroreductases confer innate niclosamide resistance in E. coli

To investigate the mechanisms by which *Escherichia coli* mitigates the antibiotic potential of niclosamide, we first examined multidrug efflux pumps, a dominant *E. coli* resistance mechanism to expel toxic compounds (33). We tested a variety of *E. coli* strains that lacked individual components of the three major tripartite efflux systems to ascertain whether efflux contributed to niclosamide resistance. In total, nine individual gene deletions were investigated for their effect on niclosamide minimal inhibitory concentration (MIC) (Table S1). Notably, deletion of the gene encoding the outer membrane channel TolC (Δ*tolC*) reduced MIC by >64-fold (MIC = 0.5 $\mu g.mL^{-1}$), whereas no other deletions had any effect (MIC >32 $\mu g.mL^{-1}$; Table S1). This result suggests that TolC-mediated efflux is one of the predominant mechanisms of niclosamide resistance. Interestingly, deletion of genes encoding other components of the principal RND-type TolC tripartite complex (AcrA or AcrB) had no effect on MIC. This was likely due to TolC interacting with alternative efflux components such as AcrE or AcrF, resulting in alternative niclosamide-capable pump assemblies (33).

Next, we explored the role of azo- and nitro-reductase flavoenzymes in niclosamide susceptibility, due to their importance in diverse metabolic pathways including antibiotic metabolism (34, 35). Although previous antibiotic metabolism studies have primarily focused on the bioreductive activation of nitro-prodrugs, we considered there was potential for nitroreduction to here be a detoxifying mechanism, as there is evidence that the nitro-moiety of niclosamide is an important structural feature for uncoupling activity (36). To

139 test this, we generated an *E. coli* strain that lacked seven flavoenzyme genes with confirmed
140 or putative nitro- or azo-reductase activity (Δ7NR) (37) (Table S1). Although niclosamide
141 resistance in Δ7NR did not change compared to wild type *E. coli* (MIC >32 μg.mL^{-1}), an
142 otherwise isogenic strain that also lacked TolC (Δ7NR*tolC*) was 2000-fold more
143 susceptible to niclosamide than wild type (MIC = 0.016 μg.mL^{-1}) and 32-fold more
144 susceptible than Δ*tolC* (**Fig. 1b**; Table S1). The relative contributions of each of the seven
145 flavoenzymes were delineated by individually overexpressing the corresponding genes in
146 Δ7NR*tolC* and investigating their effects on niclosamide IC_{50} (the concentration of
147 niclosamide required to reduce the bacterial burden by 50%). We demonstrated that three
148 enzymes, NfsA, NfsB, and AzoR, increased niclosamide IC_{50} by 10- to 15-fold (**Fig. 1c**).
149 Although these three enzymes derive from two distinct structural folds, they are all
150 proficient nitroreductases (37). Increasing nitroreductase activity could therefore be a
151 potential adaptive strategy for bacteria to develop resistance against niclosamide. We
152 hypothesized, however, that this might cause collateral sensitivity to nitroaromatic prodrug
153 antibiotics such as nitrofurantoin or metronidazole. To test this hypothesis, we selected
154 Δ7NR*tolC* cells expressing different NfsA variants (generated via multisite saturation
155 mutagenesis to combinatorically randomize seven active site residues) for resistance to
156 either 0.2 or 2μg.mL-1 niclosamide, then counter screened for sensitivity to nitrofurantoin
157 or metronidazole. Consistent with our hypothesis, increasing niclosamide resistance via
158 more proficient nitroreductase variants concomitantly decreased nitrofurantoin and
159 metronidazole resistance (**Fig. 1d-e**).

160

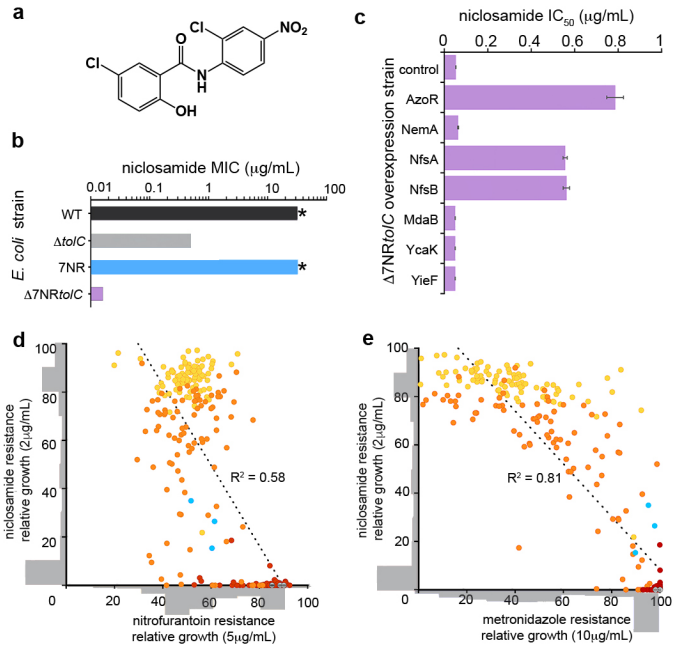

Fig. 1 | Niclosamide resistance mechanisms. a, Structure of niclosamide. **b**, MIC of *E. coli* strains: wild type (WT), Δ*tolC*, Δ7NR, and Δ7NR*tolC*; * indicates >32 μg.mL^{-1}, which is the solubility limit of niclosamide in growth media. **c,** IC_{50} analysis of Δ7NR*tolC* strains individually overexpressing candidate *E. coli* nitroreductases or a vector only control following niclosamide administration. Error bars indicate SEM. **d-e**, Covariance plots displaying the interrelated profiles of niclosamide, metronidazole or nitrofurantoin resistance. 90 colonies of NfsA variants were picked from agar plates without niclosamide (red), 0.2 μg.mL^{-1} niclosamide (orange), or 2 μg.mL^{-1} niclosamide (yellow). Variants were grown overnight and then screened for niclosamide resistance (growth at 2 μg.ml^{-1}) and (**d**) nitrofurantoin or (**e**) metronidazole resistance (growth at 5 and 10 μg.ml^{-1}, respectively). Variant distribution is shown as grey histograms that are overlaid on the x and y axes. R^2 values (linear regression analysis) are displayed; $p < 0.01$. *E. coli* NfsA and vector-only controls are displayed in cyan and grey, respectively. All panels are constructed from pooled data from at least three independent biological replicates.

Niclosamide disrupts oxidative phosphorylation in E. coli

Next, the underlying mechanisms of niclosamide antibiotic activity were investigated. As previous studies have demonstrated that niclosamide uncouples oxidative phosphorylation in mitochondria and *H. pylori* (18, 24), multiple physiological attributes were explored that

relate to this process in Gram-negative bacteria, namely proton motive force (PMF), oxygen consumption, ATP production, and redox homeostasis. The PMF has two parameters: the electric potential ($\Delta\Psi$) and the transmembrane proton (ΔpH) gradients. First, the effect of niclosamide on PMF-dissipation was investigated in EDTA-permeabilized *E. coli* using a fluorescent assay that employs the membrane potential sensitive dye $diSC_3(5)$ - a caged cation that distributes in the membrane according to $\Delta\Psi$ and self-quenches. We observed that niclosamide specifically dissipated the $\Delta\Psi$ (Fig. 2a) as revealed by de-quenching of $diSC_35$ fluorescence.

To confirm this result, checkerboard assays (dose response growth assays using serial dilutions of two drugs in combination) were performed in Δ7NR*tolC* using niclosamide and antibiotics that rely upon either $\Delta\Psi$ or ΔpH for cell uptake (kanamycin and tetracycline, respectively). The fractional inhibitory concentration index is frequently used to characterize drug interactions, but has limitations when analyzing compounds for which an individual MIC cannot be obtained (here, niclosamide). Thus, drug interactions were analyzed via Zero Interaction Potency (ZIP) scores (δ) that quantify the change in dose–response curves between individual drugs and combinations thereof, from the expectation of no interaction; δ scores >0 indicate synergism, 0 indicates no interaction, and <0 antagonism (38). Kanamycin efficacy was reduced in the presence of niclosamide, *i.e.*, niclosamide was antagonistic when co-administered with kanamycin, corresponding to a δ score of -8.2 (**Fig. 2b**), which is consistent with $\Delta\Psi$ dissipation undermining $\Delta\Psi$-dependent kanamycin uptake. In contrast, tetracycline efficacy was not affected by niclosamide co-administration (δ = 0.0; Fig. 2c), as tetracycline relies upon ΔpH for uptake (**Fig. 2b-c**). PMF disruption can reduce ATP production and increase both oxygen consumption and oxidative stress (39). We therefore confirmed that niclosamide administration significantly increased oxygen consumption in Δ7NR*tolC* (by 1.4- and 1.6-fold after administration of 60 $ng.mL^{-1}$ and 120 $ng.mL^{-1}$ niclosamide, respectively; **Fig. 2d**). Niclosamide administration caused a reduction of cellular ATP concentration to 3% and 1% of DMSO-control concentrations when 4 $\mu g.mL^{-1}$ niclosamide was administered to Δ*tolC* and Δ7NR*tolC*, respectively (**Fig. 2e**). Employing strains constitutively expressing redox-sensitive GFP (40), we determined that niclosamide also disrupted redox homeostasis in

212 Δ*tolC* and Δ7NR*tolC* strains, causing an increase in oxidative stress (**Fig. 2f-g**; Fig. S1).
213 Next, using high-throughput fluorescence microscopy, increased intracellular oxidative
214 stress was visualized in Δ7NR*tolC* cells following niclosamide administration. The
215 distribution of redox stress per cell was plotted as histograms (Fig. S1) and a random
216 selection of pseudo-colored ratio images are presented in **Fig. 2h**. In strains that retained
217 TolC function, niclosamide did not have a significant effect on cellular ATP levels, oxygen
218 consumption, or redox homeostasis. Taken together, these data suggest that, when efflux
219 is compromised, niclosamide dissipates the $\Delta\Psi$ to collapse the PMF and uncouple
220 oxidative phosphorylation in *E. coli*.

221

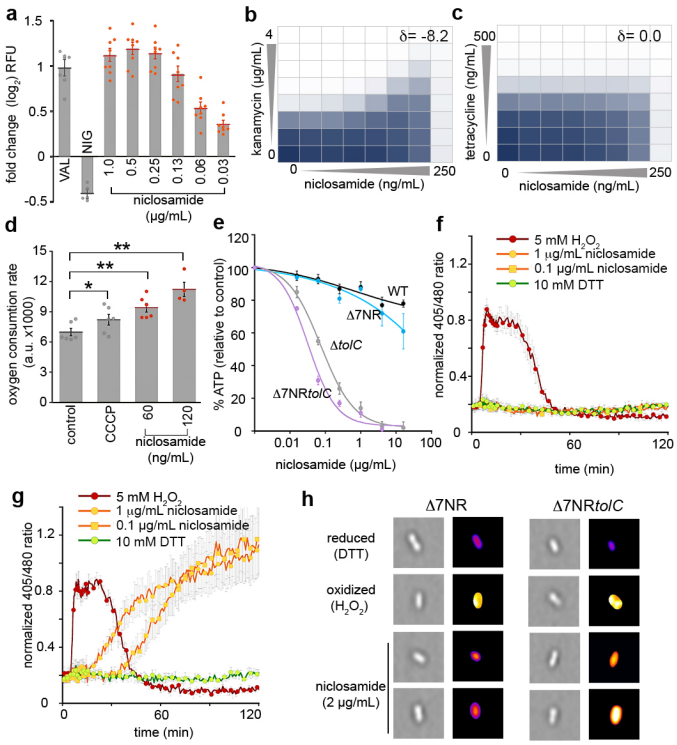

Fig. 2 | Antibiotic mechanisms of niclosamide. **a**. Fold change in $DiSC_3(5)$ fluorescence. *E. coli* was grown in MHB with 10 mM EDTA to an OD_{600} of 1. Cells were incubated with $DiSC_3(5)$ for 20 min prior to administration of 0.5 μg/mL valinomycin (VAL; a ΔΨ-dissipating ionophore), 0.5 μg/mL nigericin (NIG; a ΔpH-dissipating ionophore) or 0.03 to 1 μg/mL niclosamide. 100 mM KCl was added to cells prior to valinomycin treatment. **b-c,** The combined inhibitory effects of 0 - 250 ng.mL^{-1} niclosamide and either (**b**) 0 - 4 μg.mL^{-1} kanamycin, or (**c**) 0 - 500 ng.mL^{-1} tetracycline were tested against Δ7NR*tolC* in a checkerboard format. Bacterial growth is shown as a heat plot. **d**, Oxygen consumption was measured using the MitoXpress oxygen probe in Δ7NR*tolC* cells (mid-log; OD_{600} = 0.15) overlaid with mineral oil for 20 min. **e**, Relative cellular ATP levels were estimated by luciferase activity and compared to unchallenged (DMSO-only) control. **f-g**, Intracellular oxidation levels were measured in (**f**) WT *E. coli* and (**g**) Δ*tolC* strains constitutively expressing redox-sensitive GFP (roGFP) following administration of 5 mM H_2O_2 (oxidized control), 10 mM DTT (reduced control), or niclosamide. **h**, Representative high-throughput fluorescence microscopy images of Δ7NR and Δ7NR*tolC* cells 120 min after administration of DTT, H_2O_2, or niclosamide. Images on the right are pseudo-colored ratio images after analysis with ImageJ. Panels a-g were constructed from pooled data from at least three independent biological replicates. Labels indicate significant responses over the control (* = P<0.05; ** = P<0.01). Statistical analyses were performed using One-way ANOVA, Kruskal-Wallis test. Error bars indicate SEM.

Niclosamide synergizes with efflux pump inhibitors and membrane permeabilizers for enhanced efficacy against E. coli

After establishing the mode of action of niclosamide and the basis of Gram-negative innate resistance, we next sought to identify compounds that sensitize Gram-negative bacteria to niclosamide when administered in combination. Predicting that efflux pump inhibitors such as phenylalanine-arginine β-naphthylamide (PAβN) (41) would increase niclosamide sensitivity, checkerboard assays were employed to screen niclosamide and PAβN against *E. coli*. Considerable synergy was observed (δ = 47.9; **Fig. 3a**). It was next reasoned that increased niclosamide influx via outer membrane permeabilization might mitigate TolC-mediated efflux. Therefore, membrane permeabilizing polymyxin antibiotics were investigated for synergy and, consistent with recent reports (29-31), synergy was observed when colistin or polymyxin B were co-administered with niclosamide (δ = 28.1 and 25.6, respectively) (**Fig. 3b-c**). We hypothesized that synergism was due to the cascading effect of the mode of action of niclosamide, in that polymyxins increased the influx of niclosamide and thereby facilitated PMF dissipation, which in turn compromised the efficiency of PMF-dependent niclosamide efflux (as efflux was dependent upon PMF (42)). Ultimately, this would result in higher intracellular concentrations of niclosamide and thus enhanced antibiotic effects (Fig. S2). Indeed, polymyxin synergy was less evident in Δ*tolC* (δ = 7.6 and 9.7 for colistin and polymyxin B respectively; **Fig. 3d-e**) and niclosamide administration inhibited efflux in EDTA-permeabilized *E. coli* (observed via increasing intracellular accumulation of the fluorescent nucleic acid probe Hoechst 33342; Fig. S1).

Oxyclozanide potentiates diverse antibiotics, likely via inhibition of PMF-dependent efflux

Next, it was examined whether the synergistic relationships observed above were maintained for other halogenated salicylanilides, namely oxyclozanide, closantel, and rafoxanide. It was confirmed that all these niclosamide analogs synergized with both PAβN and colistin (δ = 21.5 to 49.8; **Fig. 3f**; Fig. S3). Of note, the relatively high solubility of oxyclozanide in growth media (~512 $\mu g.mL^{-1}$), compared to that of other salicylanilides (~64 $\mu g.mL^{-1}$), enabled the observation of an oxyclozanide MIC (256 $\mu g.mL^{-1}$), *i.e.*,

sufficiently high concentrations of oxyclozanide could overcome TolC-mediated efflux. Since moderate synergistic relationships can only be detected at concentrations nearing the MIC of both drugs and are emphasized in bacterial cultures under nutrient limitation (43), oxyclozanide checkerboard assays in minimal media were used to identify additional antibiotics that interact with salicylanilides against *E. coli*. Twelve antibiotics with diverse cellular targets (Table S1) were examined. Interestingly, 6 out of 12 antibiotics synergized with oxyclozanide (chloramphenicol, tetracycline, cefotaxime, meropenem, ciprofloxacin, and nitrofurantoin; δ = 5.7 to 10.8), five antibiotics displayed no or weak interactions (δ = -0.6 to 2.9) and, consistent with the dependence of aminoglycosides on $\Delta\Psi$ for uptake, oxyclozanide antagonized gentamicin activity (δ = -6.3) (**Fig. 3g**; Table S2; **Fig. 4**). These combinatorial effects were neutralized or reversed when examined in the Δ*tolC* strain (**Fig. 3g**; Table S2; **Fig. 4**) and oxyclozanide synergy was typically stronger for antibiotics that are TolC-substrates (indicated by fold IC_{50} change in Δ*tolC* compared to *E. coli*; **Fig. 3h**). These results suggest that oxyclozanide synergy might be at least partially underpinned by the inhibition of efflux via PMF dissipation (Fig. S2). To substantiate this hypothesis, the effect of oxyclozanide on cellular efflux was examined using Hoechst 33342. Indeed, administration of oxyclozanide inhibited efflux (**Fig. 3i**). Taken together, these results demonstrate that chemical disruption of TolC-mediated efflux or membrane integrity sensitizes *E. coli* to salicylanilides. Further studies are required to explain detailed drug interactions, however, our results suggest that PMF-dissipating compounds such as salicylanilides may potentiate the activity of diverse antibiotics through the disruption of efflux.

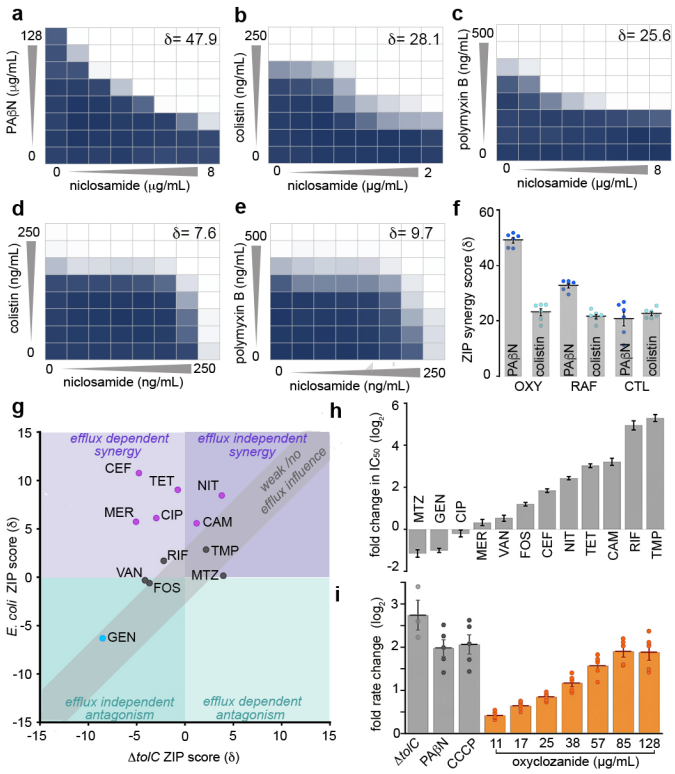

Fig. 3 | Analyses of salicylanilide synergy interactions. a-c, The combined inhibitory effects of 0 - 8 μg.mL^{-1} niclosamide and either (**a**) 0 - 128 μg.mL^{-1} PAβN, or (**b**) 0 - 250 ng.mL^{-1} colistin, or (**c**) 0 – 500 ng.mL^{-1} polymyxin B were tested against *E. coli* using checkerboard analysis. ZIP synergy scores (δ) are presented. Bacterial growth is depicted as a heat plot. **d-e**, The combined inhibitory effects of 0 to 250 ng.mL^{-1} niclosamide and either (**d**) 0 to 250 ng.mL^{-1} colistin or (**e**) 0 – 500 ng.mL^{-1} polymyxin B were tested against *E. coli* Δ*tolC* in checkerboard analyses. Bacterial growth is depicted as a heat plot. **f**, A bar graph of ZIP scores (δ) depicting the synergism of oxyclozanide (OXY), rafoxanide (RAF), or closantel (CTL) in combination with PAβN or colistin against *E. coli*. Error bars indicate SEM. **g-h**, Analysis of oxyclozanide synergy with: nitrofurantoin (NIT), metronidazole (MTZ), cefotaxime (CEF), rifampicin (RIF), tetracycline (TET), gentamicin (GEN), ciprofloxacin (CIP), chloramphenicol (CAM), trimethoprim (TMP), fosfomycin (FOS), meropenem, (MER) or vancomycin (VAN). (**g**) A covariance plot of antibiotic ZIP scores from checkerboard assays conducted in minimal media with oxyclozanide against *E. coli* and Δ*tolC*. (**h**) A bar chart displaying the fold change of IC_{50} values in *E. coli* compared to Δ*tolC*; uncertainty is indicated by error bars. **i**, Fold change in rate of H33342 fluorescence (compared to a DMSO control) in Δ*tolC* cells or WT *E. coli* following administration of 28 μg.mL^{-1} PAβN, 5 μg.mL^{-1} CCCP, or 11.2 to 128 μg.mL^{-1} oxyclozanide. Error bars indicate SEM. All panels were constructed from pooled data from at least three independent biological replicates.

315 ***Niclosamide/colistin combination therapy is effective against diverse clinical Gram-***
316 ***negative isolates in vitro and in vivo***

317 Finally, we investigated the potential of salicylanilide combination therapy against a range
318 of Gram-negative clinical isolates. Due to the immediate repurposing potential of
319 niclosamide as an FDA-approved clinical drug and increasing concerns around colistin-
320 resistant pathogens, we prioritized these two compounds. Checkerboard assays were
321 performed on nine MDR clinical isolates across diverse phyla: *Acinetobacter*,
322 *Pseudomonas* and the *Enterobacteriaceae* (Table S3). Co-administration of niclosamide
323 and colistin yielded synergistic efficacy in all strains including the colistin resistant clinical
324 isolate, *P. aeruginosa* LESB58 (δ = 8.4 to 36.7), enabling up to 4-fold lower doses of
325 colistin (**Fig. 4a;** Fig. S5), which is of particular importance due to the nephrotoxicity
326 issues associated with this antibiotic (44).

327 The poor bioavailability and pharmacology of niclosamide may be mitigated via local
328 administration, *e.g.*, topical or inhalation therapies (28, 45). Here, we examined the *in vivo*
329 antibacterial synergy of niclosamide via direct injection in a high-density murine cutaneous
330 infection model that mimics clinical situations where antibiotic treatments are typically
331 unsuccessful, *e.g.,* skin abscesses (32) (**Fig. 4b**). The synergistic efficacy of niclosamide
332 and colistin was validated against *P. aeruginosa* LESB58 and *K. pneumoniae* KPLN649.
333 Co-administration resulted in significant synergistic efficacy against both strains, reducing
334 the *K. pneumoniae* and *P. aeruginosa* bacterial load by 32- and 12-fold, respectively, over
335 the sum of the individual therapies, and by 239- and 19-fold, respectively, when compared
336 to vehicle-only controls (**Fig. 4c-d**). This is the first report of *in vivo* efficacy for
337 niclosamide and colistin against Gram-negative pathogens, and notably, this was achieved
338 against recalcitrant high-density infections for which no effective clinical treatments
339 currently exist (32). It is also important to note that this study was focused on detecting
340 niclosamide/colistin synergy rather than identifying the best formulation or dose ratio for
341 efficacy; more significant efficacy could likely be achieved by optimising the drug
342 concentrations or dosing regimen.

343

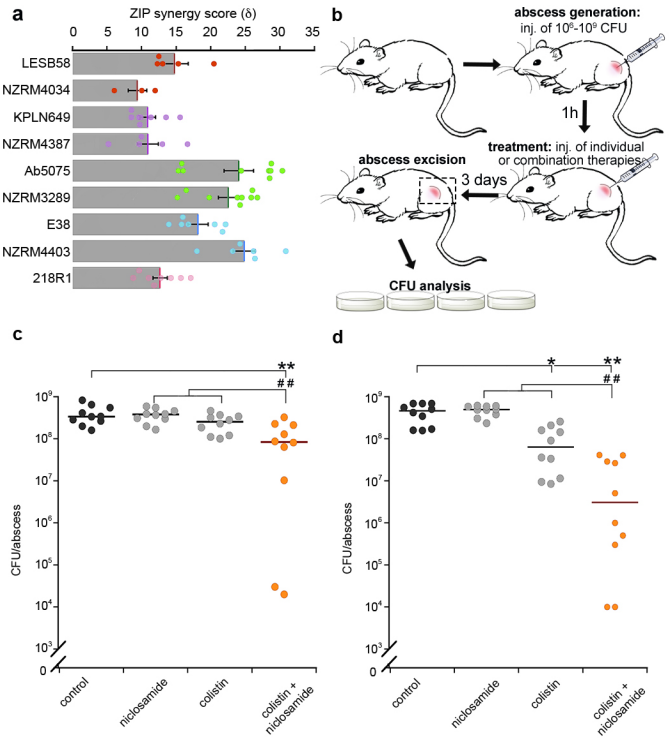

Fig. 4 | Niclosamide/colistin combination therapy was effective against recalcitrant MDR Gram-negative strains. a, Bar graph depicting *in vitro* ZIP scores (δ) of niclosamide and colistin co-administration against clinical MDR Gram-negative strains: *P. aeruginosa* LESB58, *P. aeruginosa* NZRM4034, *K. pneumoniae* KPLN649, *K. pneumoniae* NZRM4387, *A. baumannii* Ab5075, *A. baumannii* NZRM3289, *E. coli* E38, *E. coli* NZRM4403 and *E. cloacae* 218R1. The ZIP synergy score (δ) is presented as the average interaction from an 8×8 dose-response matrix. Data was averaged from at least three independent experiments and error bars indicate SEM. **b**, Diagram of abscess model procedure and analysis. **c-d**, Dot plots of (**c**) colistin-resistant *P. aeruginosa* LESB58 and (**d**) *K. pneumoniae* KPLN649 survival, represented as CFUs recovered per abscess after administration of 10 $mg.kg^{-1}$ niclosamide ethanolamine salt and 0.15 $mg.kg^{-1}$ (*P. aeruginosa*) or 2.5 $mg.kg^{-1}$ (*K. pneumoniae*) colistin as individual or combined therapeutics. Labels indicate: significant responses over the PEG control (*, $p < 0.05$; **, $p < 0.01$); or synergistic responses, *i.e.*, significant differences of the combination therapy over the sum of the effects of each agent alone ($^{\#\#}$, $p < 0.01$). Statistical analyses were performed using One-way ANOVA, Kruskal-Wallis test with Dunn's correction (two sided).

Discussion

By harnessing a diverse set of biochemical and genetic tools, this work explores the Gram-negative antibacterial potential of niclosamide and related salicylanilide analogs. We reveal

the molecular action of salicylanilides against Gram-negative bacteria, detailing not only the underlying mechanisms of antibiotic activity, but also the basis for innate and adaptive resistance and the mechanisms that underpin the synergies between salicylanilides and a diversity of other antibiotics. These data enabled the development of a model that substantially advances our knowledge of the physiological effects of salicylanilides in Gram-negative bacteria (Fig. S2). Efflux is an established Gram-negative resistance mechanism and indeed, this is the predominant basis for niclosamide resistance. However, we demonstrate that salicylanilides also inhibit efflux and thus synergize with a wide range of antibiotics for which efflux is a common resistance mechanism. These data highlight the potential of the salicylanilide chemical scaffold, and PMF-dissipating compounds in general, for the discovery and design of novel antibiotic adjuvants to address efflux-mediated resistance. We consider PMF-dissipation, traditionally avoided in early drug development due to presumed toxicity, a promising and unexplored trait for the development of antimicrobials (46). Interestingly, many clinical compounds for diverse medical purposes have been reported to have mild PMF-dissipating activity and in addition, some have displayed antibiotic efficacy against Gram-positive or acid-fast pathogens such as *S. aureus* and *M. tuberculosis* (46, 47). Gram-negative pathogens, in contrast resist the action of such compounds via their robust cellular envelope and diverse efflux pumps (33). Co-administration of PMF-dissipating compounds with drugs that target efflux and cell permeability may therefore be a promising avenue to discover more effective combination therapies. Combining mechanistic insights with previously established data around safety and pharmacology for repurposed "non-antibiotic" clinical compounds may rapidly identify attractive candidates for accelerated clinical development.

Understanding the evolutionary basis of antibiotic resistance is important to inform the sustainable use of next generation antibiotics. Due to the failure of laboratory evolution experiments to generate niclosamide resistance in *S. aureus* or *H. pylori*, previous reports have suggested that a key advantage of niclosamide as a potential antimicrobial is the apparent lack of resistance mechanisms (24, 45). We show, however, that nitroreductases inactivate niclosamide to reduce antibiotic toxicity and enhanced nitroreductase activity can cause niclosamide resistance. While modulation of nitroreductase activity is a known Gram-negative resistance mechanism against nitro-antibiotic compounds, this is typically

caused by null mutations, *i.e.*, a genetic change that results in a non-functional nitroreductase, to prevent the activation of prodrug antibiotics such as metronidazole (48). Our results suggest that resistance has potential to emerge in the clinic through enhanced nitroreductase activity. Significantly, we show that this may result in collateral sensitivity to nitroimidazole antibiotics, and thus propose a strategy to mitigate this evolutionary route, *i.e.* cyclic treatments of metronidazole. This demonstrates how mechanistic understanding can accelerate not only the discovery, but also potentially the sustainability of new Gram-negative combination therapies.

In summary, we reveal the detailed mechanisms that underlie the antibiotic mode of action, routes of resistance and synergistic relationships of salicylanilides. This guided the discovery of novel combination therapies and emphasizes how mechanistic understanding is critical when seeking to repurpose clinical compounds. Salicylanilides, and likely other PMF-dissipating compounds, may have broad utility as Gram-negative antibiotics in combination therapies.

Acknowledgements

This work was supported by the Royal Society of New Zealand Marsden Fund (grant VUW1502 to D.F.A.), the Health Research Council of New Zealand (18-532 to D.F.A.), a Natural Sciences and Engineering Research Council of Canada Discovery Grant (RGPIN 2017-04909 to N.T.) and a Canadian Institutes for Health Research (CIHR) grant (FDN-154287 to R.E.W.H.). D.P. received a Cystic Fibrosis Postdoctoral Fellowship (Canada) and a Research Trainee Award from the Michael Smith Foundation for Health Research. R.E.W.H. holds a Canada Research Chair in Health and Genomics and a UBC Killam Professorship. N.T. is a CIHR new investigator and a Michael Smith Foundation of Health Research career investigator. J.N.C. thanks Jaiten Saini for technical support.

Author contributions

J.N.C. and D.F.A. designed and directed the project, and co-wrote the manuscript. J.N.C performed the mechanistic studies and bacterial screening assays. N.T. assisted project design and co-wrote the manuscript. J.V.D.H. performed the AMNIS high throughput screening and assisted intracellular redox assays; M.H.R., A.S.B., R.F.L., C.M.M. and R.J.E. assisted bacterial screening; E.M.W. provided experimental support for molecular engineering and bacterial assays; D.P. carried out all abscess infection studies; D.P and R.E.W.H. directed the mouse abscess infection studies and assisted in manuscript editing.

Declaration of Interests

J.N.C. and D.F.A. are co-inventors on patent filings WO/2016/080846 and WO/2017/200396 for the application of niclosamide, and related compounds, in conjunction with efflux inhibitors or membrane permeabilizing agents. Some of the claims in these filings are supported by this work.

Methods

Bacterial Strains: *E. coli* BW25113 strains bearing individual gene deletions were obtained from the Keio knockout collection (49). Δ7NR and Δ7NR*tolC* were generated via sequential knockout as previously described (50). New Zealand clinical isolates used in this study were *A. baumannii* NZRM3289, *P. aeruginosa* NZRM4034, *K. pneumoniae* NZRM4387 and *E. coli* NZRM4403 (obtained from the New Zealand Reference Culture Collection, Environmental Science and Research Ltd.), additional strains, *K. pneumoniae* KPLN649, *A. baumannii* Ab5075, *P. aeruginosa* LESB58, *E. cloacae* 218R1, *E. coli* E38 (Serotype O78:H^-) (BEI resources, NR-17717) as previously described (51).

In vitro growth analyses: Minimal inhibitory concentrations (MIC) were determined using two-fold dilutions and growth was measured after 16 - 48 h (52). The MIC was the concentration that inhibited growth >90% when compared to controls. DMSO was present at a final concentration of 2.5 % unless otherwise stated. For checkerboard analysis, an 8 × 12 matrix was created with two-fold serial dilutions of each compound. Bacterial colonies were isolated from a freshly streaked plate and resuspended in MHB media for OD_{600} normalization. After addition of bacteria to a final OD_{600} of 0.001, checkerboard plates were incubated at 30 °C with shaking for 16 h (or 36 h at 37 °C for *P. aeruginosa* strains), at which time the OD_{600} was measured. Checkerboard assays in minimal media were typically performed at 37 °C (oxyclozanide checkerboard assays with nitrofurantoin, rifampicin, tetracycline and chloramphenicol were performed at 30 °C) with shaking for 16 h, from a starting OD_{600} of 0.04. For the analysis of nitroreductase overexpression strains, individual colonies were transferred via nitrocellulose membrane to an agar plate containing 1mM IPTG and incubated for 3.5 h. IPTG-induced cells were then removed from the membrane and resuspended in MHB media for checkerboard analysis as described above. Relative IC_{50} values (the concentration of the compound required to reduce the bacterial burden by 50% compared to unchallenged controls) were calculated from the dose-response curves using the four-parameter equation y=m1+(m2-m1)/(1+(x/m3)^m4) determined by Kaleidagraph software (Synergy Software, Reading, PA) where m1 = lower asymptote, m2 = lower asymptote, m3 = relative IC_{50}, and m4 = slope.

Generation and screening of mutagenized NfsA variants: A plasmid-based multisite saturation mutagenesis library of *E. coli* NfsA (UniProtKB ID: P17117) was generated via combinatorial randomization of the codons encoding seven key active site residues: S41, F42, F83, K222, S224, R225 and F227 (Fig. S6). All codons were randomized to NDT (a degeneracy that specifies a balanced range of 12 different amino acids including the native residue), with the exception of position 222, which was randomized to NNK (specifying all 20 possible amino acids). The resulting library of nearly 96 million codon variants was expressed in Δ7NR*tolC*. To analyze the activity of NfsA variants, library subsets were selected on agar plates using 0, 0.2 and 2 $\mu g.mL^{-1}$ of niclosamide. Ninety colonies from each subset were subsequently screened via growth assays with niclosamide, metronidazole, and nitrofurantoin at 2, 10, and 5 $\mu g.mL^{-1}$ respectively; growth was measured via OD_{600} following 4 h incubation as previously described (53).

Synergy Calculations: For each checkerboard analysis, an 8 × 8 matrix of averaged checkerboard results from at least three (typically >5) independent experiments was used to calculate ZIP scores using SynergyFinder (Bioconductor.org) (38, 54).

$DiSC_3(5)$ assay: Subcultures of *E. coli* BW25113 were grown to late exponential phase (OD_{600} ~1) in MHB with 10 mM EDTA (to facilitate $DiSC_3(5)$ cell entry). Cells were harvested by centrifugation, washed twice in buffer (5 mM HEPES, pH 7.2, 20 mM glucose, 5% DMSO), and then resuspended in buffer to a final OD_{600} = 0.085 with 1 μM DiSC3(5). For valinomycin, 100 mM KCl was added to the cell suspension containing $DiSC_3(5)$. After a 20 min incubation at 37 °C, 190 μL of $DiSC_3(5)$ loaded cells were added to two-fold dilutions of niclosamide, valinomycin, or nigericin in 96-well black clear-bottom plates (Corning, NY). Fluorescence (Ex: 620 nm, Em: 685 nm) was immediately read using a Synergy H1 Hybrid plate reader.

Measurement of intracellular ATP levels: *E. coli* BW25113 was grown in MHB to early-log phase (OD_{600} = 0.2) and then grown in the presence of niclosamide or CCCP for 60 min in clear flat-bottom 96-well plates. The OD_{600} was determined immediately before ATP levels were measured using BacTiter-Glo™ (Promega, Madison WI), according to

491 manufacturer instructions. Relative ATP levels were calculated by dividing relative light
492 units (RLU) by the OD_{600} (RLU/OD).

493 ***Measurement of Oxygen consumption:*** *E. coli* strains were grown in MHB to early-log
494 phase (OD_{600} = 0.4) before dilution to OD_{600} = 0.1 prior to the assay. 50 µL of diluted
495 culture was added to individual wells of a 96-well black clear-bottom plate (Corning, NY)
496 containing 5 µL of a DMSO control, CCCP, or niclosamide at the desired concentration,
497 and 5 µL of the MitoXpress oxygen probe. Cells were immediately covered with a layer of
498 high-sensitivity mineral oil (50 µL) to restrict oxygen diffusion. Fluorescence (Ex: 380 nm,
499 Em: 650 nm) was recorded using a Synergy H1 Hybrid plate reader.

500 ***Measurement of bacterial efflux:*** Subcultures of *E. coli* BW25113 were grown to early
501 exponential phase (OD_{600} ~0.4) in MHB supplemented with 5 mM EDTA, harvested by
502 centrifugation, and resuspended in PBS to a final OD_{600} = 0.1. To initiate accumulation
503 assays, Hoescht 33342 was added (1µM), cells were mixed by inversion and 150 µl aliquots
504 were added in a black, clear-bottom 96-well plate containing 50 µL of oxyclozanide,
505 niclosamide, PAβN or CCCP at 4× the desired concentration(s) in PBS with 20% DMSO.
506 Fluorescence (Ex: 355 nm, Em:460 nm) was measured for 10 min using a Synergy H1
507 Hybrid plate reader (55).

508 ***Measurement of intrabacterial redox potential***: roGFP contains an intramolecular
509 disulfide bond that induces a shift in fluorescence emission between 405 nm and 480 nm,
510 thus intracellular oxidative stress can be ratiometrically monitored. *In vitro* analysis of the
511 intrabacterial redox potential was performed as previously published (40) Assays were
512 performed at 30 °C in a Synergy H1 Hybrid plate reader with excitation measured at 405
513 and 480 nm, and emission at 510 nm. Log phase bacterial cultures were resuspended in
514 0.9% sodium chloride at OD_{600} of 1.0, and 180 µL per well were loaded in a black, clear-
515 bottom 96-well plate. The signals for fully oxidized or fully reduced bacteria were obtained
516 by adding 5 mM H_2O_2 or 10 mM DTT to the bacteria culture at the start of the experiment.
517 Niclosamide was added at 1 and 0.1 $\mu g.mL^{-1}$. All values were normalized to the values
518 obtained for maximally oxidized and for fully reduced bacterial cultures.

519 ***AMNIS ImageStream and IDEAS/ImageJ Analysis***: Samples were analysed by the
520 AMNIS ImageStream as previously described (40). The laser intensities for 405, 488, 658,
521 and 785 nm were 100, 120, 20, and 3.8, respectively. The data files were further analysed
522 with the IDEAS software, version 6.0.129.0, which is supplied by AMNIS. Bacterial cells
523 were selected based on fluorescence at 660 nm. Every cell image was then selected by the
524 program based on fluorescent intensity at 660 nm. A mask was then created for analysis of
525 the 405/480 nm ratio. The resulting 405/480 signals were plotted in a histogram. Reduced
526 and oxidized controls were obtained within each experiment, niclosamide was
527 administered at 2 $\mu g.mL^{-1}$. All values were normalized to oxidized and reduced ratio
528 values. Pseudo-colored ratio images were generated by ImageJ as described previously
529 (40).

530 ***Murine abscess infection studies***: Animal experiments were performed in accordance with
531 The Canadian Council on Animal Care (CCAC) guidelines and were approved by the
532 University of British Columbia Animal Care Committee (certificate number A14-0363).
533 Mice used in this study were female outbred CD-1. All animals were purchased from
534 Charles River Laboratories (Wilmington, MA), were 7 weeks of age, and weighed 25 ± 3
535 g at the time of the experiments. 1 to 3% isoflurane was used for anesthesia. Mice were
536 euthanized with carbon dioxide. The abscess infection model was performed as previously
537 described (51). *K. pneumoniae* KPLN649 and *P. aeruginosa* LESB58 were grown to an
538 OD_{600} of 1.0 in dYT broth. Prior to injection, bacterial cells were washed twice with sterile
539 PBS and resuspended to 5×10^7 CFU for *P. aeruginosa* LESB58 and 1×10^9 CFU for *K.*
540 *pneumoniae* KPLN49. A 50 µl bacterial suspension was injected into the right side of the
541 dorsum. Up to 10 $mg.kg^{-1}$ niclosamide and 5 $mg.kg^{-1}$ colistin, each dissolved in 2.5%
542 DMSO, 42.5% PEG400, were tested for skin toxicity prior to efficacy testing. Treatment
543 was applied directly into the subcutaneous space into the infected area (50 µl) at 1 h post
544 infection. The progression of the disease/infection was monitored daily and skin abscesses
545 were excised (including all accumulated pus) on day three, homogenized in sterile PBS
546 using a Mini-Beadbeater-96 (Biospec products, Bartlesville, OK) for 5 min and bacterial
547 counts determined by serial dilution. Experiments were performed at least 3 times
548 independently with 3 to 4 animals per group.

549 ## References

550 1. **World Health Organization**. 2017. Global priority list of antibiotic-resistant
551 bacteria to guide research, discovery, and development of new antibiotics. WHO.
552 1-7.

553 2. **Tyers M**, **Wright GD**. 2019. Drug combinations: a strategy to extend the life of
554 antibiotics in the 21st century. Nat Rev Micro **17**:141–155.

555 3. **Zimmer A**, **Katzir I**, **Dekel E**, **Mayo AE**, **Alon U**. 2016. Prediction of
556 multidimensional drug dose responses based on measurements of drug pairs. Proc
557 Natl Acad Sci USA **113**:10442–10447.

558 4. **Yeh P**, **Tschumi AI**, **Kishony R**. 2006. Functional classification of drugs by
559 properties of their pairwise interactions. Nat Genet **38**:489–494.

560 5. **Zuo GY**, **Li Y**, **Wang T**, **Han J**, **Wang GC**, **Zhang YL**, **Pan WD**. 2011.
561 Synergistic antibacterial and antibiotic effects of bisbenzylisoquinoline alkaloids
562 on clinical isolates of methicillin-resistant *Staphylococcus aureus* (MRSA).
563 Molecules **16**:9819–9826.

564 6. **Mitchison DA**. 2012. Prevention of drug resistance by combined drug treatment of
565 tuberculosis. Handb Exp Pharmacol **211**:87–98.

566 7. **Vidaillac C**, **Benichou L**, **Duval RE**. 2012. In Vitro Synergy of Colistin
567 Combinations against Colistin-Resistant *Acinetobacter baumannii*, *Pseudomonas*
568 *aeruginosa*, and *Klebsiella pneumoniae* Isolates. Antimicrob Agents Chemother
569 **56**:4856–4861.

570 8. **Foucquier J**, **Guedj M**. 2015. Analysis of drug combinations: current
571 methodological landscape. Pharmacol Res Perspect **3**:e00149.

572 9. **Tooke CL**, **Hinchliffe P**, **Bragginton EC**, **Colenso CK**, **Hirvonen VHA**,
573 **Takebayashi Y**, **Spencer J**. 2019. β-Lactamases and β-Lactamase Inhibitors in the
574 21st Century. J Mol Biol **431**:3472–3500.

575 10. **Minato Y**, **Dawadi S**, **Kordus SL**, **Sivanandam A**, **Aldrich CC**, **Baughn AD**.
576 2018. Mutual potentiation drives synergy between trimethoprim and
577 sulfamethoxazole. Nat Comms **9**:1003.

578 11. **Lehtinen J**, **Lilius EM**. 2007. Promethazine renders *Escherichia coli* susceptible
579 to penicillin G: real-time measurement of bacterial susceptibility by fluoro-
580 luminometry. Int J Antimicrob Agents **30**:44–51.

581 12. **Kristiansen JE**, **Hendricks O**, **Delvin T**, **Butterworth TS**, **Aagaard L**,
582 **Christensen JB**, **Flores VC**, **Keyzer H**. 2007. Reversal of resistance in
583 microorganisms by help of non-antibiotics. J Antimicrob Chemother **59**:1271–
584 1279.

13. **Ejim L**, **Farha MA**, **Falconer SB**, **Wildenhain J**, **Coombes BK**, **Tyers M**, **Brown ED**, **Wright GD**. 2011. Combinations of antibiotics and nonantibiotic drugs enhance antimicrobial efficacy. Nat Chem Biol **7**:348–350.

14. **Konreddy AK**, **Rani GU**, **Lee K**, **Choi Y**. 2018. Recent Drug-Repurposing-Driven Advances in the Discovery of Novel Antibiotics. Curr Med Chem **25**.

15. **Stokes JM**, **MacNair CR**, **Ilyas B**, **French S**, **Côté J-P**, **Bouwman C**, **Farha MA**, **Sieron AO**, **Whitfield C**, **Coombes BK**, **Brown ED**. 2017. Pentamidine sensitizes Gram-negative pathogens to antibiotics and overcomes acquired colistin resistance. Nat Microbiol **2**:17028.

16. **Ditzel J**, **Schwartz M**. 1967. Worm cure without tears. The effect of niclosamide on *Taeniasis saginata* in man. J Intern Med **182**:663–664.

17. **Chen W**, **Mook RA**, **Premont RT**, **Wang J**. 2018. Niclosamide: Beyond an antihelminthic drug. Cell Signal **41**:89–96.

18. **Weinbach EC**, **Garbus J**. 1969. Mechanism of action of reagents that uncouple oxidative phosphorylation. Nature **221**:1016–1018.

19. **Kadri H**, **Lambourne OA**, **Mehellou Y**. 2018. Niclosamide, a Drug with Many (Re)purposes. ChemMedChem **13**:1088–1091.

20. **Wu CJ**, **Jan JT**, **Chen CM**, **Hsieh HP**, **Hwang DR**, **Liu HW**, **Liu CY**, **Huang HW**, **Chen SC**, **Hong CF**, **Lin RK**, **Chao YS**, **Hsu JTA**. 2004. Inhibition of severe acute respiratory syndrome coronavirus replication by niclosamide. Antimicrob Agents Chemother **48**:2693–2696.

21. **Jeon S**, **Ko M**, **Lee J**, **Choi I**, **Byun SY**, **Park S**, **Shum D**, **Kim S**. 2020. Identification of antiviral drug candidates against SARS-CoV-2 from FDA-approved drugs. bioRxiv 2020.03.20.999730.

22. **Jurgeit A**, **McDowell R**, **Moese S**, **Meldrum E**, **Schwendener R**, **Greber UF**. 2012. Niclosamide Is a Proton Carrier and Targets Acidic Endosomes with Broad Antiviral Effects. PLoS Pathog **8**:e1002976.

23. **Rajamuthiah R**, **Fuchs BB**, **Conery AL**, **Kim W**, **Jayamani E**, **Kwon B**, **Ausubel FM**, **Mylonakis E**. 2015. Repurposing Salicylanilide Anthelmintic Drugs to Combat Drug Resistant *Staphylococcus aureus*. PLoS ONE **10**:e0124595.

24. **Tharmalingam N**, **Port J**, **Castillo D**, **Mylonakis E**. 2018. Repurposing the anthelmintic drug niclosamide to combat *Helicobacter pylori*. Sci Rep **8**:3701.

25. **Andrews P**, **Thyssen J**, **Lorke D**. 1982. The biology and toxicology of molluscicides, Bayluscide. Pharmacol Ther **19**:245–295.

26. **Lin CK**, **Bai MY**, **Hu TM**, **Wang YC**, **Chao TK**, **Weng SJ**, **Huang RL**, **Su PH**, **Lai HC**. 2016. Preclinical evaluation of a nanoformulated antihelminthic, niclosamide, in ovarian cancer. Oncotarget **7**:8993–9006.

27. **Mook RA**, **Wang J**, **Ren X-R**, **Chen M**, **Spasojevic I**, **Barak LS**, **Lyerly HK**, **Chen W**. 2015. Structure-activity studies of Wnt/β-catenin inhibition in the Niclosamide chemotype: Identification of derivatives with improved drug exposure. Bioorg Med Chem **23**:5829–5838.

28. **Costabile G**, **d'Angelo I**, **Rampioni G**, **Bondì R**, **Pompili B**, **Ascenzioni F**, **Mitidieri E**, **d'Emmanuele di Villa Bianca R**, **Sorrentino R**, **Miro A**, **Quaglia F**, **Imperi F**, **Leoni L**, **Ungaro F**. 2015. Toward Repositioning Niclosamide for Antivirulence Therapy of *Pseudomonas aeruginosa* Lung Infections: Development of Inhalable Formulations through Nanosuspension Technology. Mol Pharm **12**:2604–2617.

29. **Ayerbe-Algaba R**, **Gil-Marqués ML**, **Jiménez-Mejías ME**, **Sánchez-Encinales V**, **Parra-Millán R**, **Pachón-Ibáñez ME**, **Pachón J**, **Smani Y**. 2018. Synergistic Activity of Niclosamide in Combination With Colistin Against Colistin-Susceptible and Colistin-Resistant *Acinetobacter baumannii* and *Klebsiella pneumoniae*. Front Cell Infect Microbiol **8**:348.

30. **Domalaon R**, **De Silva PM**, **Kumar A**, **Zhanel GG**, **Schweizer F**. 2019. The anthelmintic drug niclosamide synergizes with colistin and reverses colistin resistance in Gram-negative bacilli. Antimicrob Agents Chemother **63**:e02574-18.

31. **Ackerley DF**, **Copp JN**. 2017. Antibacterial compositions. WO2016080846A1

32. **Pletzer D**, **Mansour SC**, **Wuerth K**, **Rahanjam N**, **Hancock REW**. 2017. New Mouse Model for Chronic Infections by Gram-Negative Bacteria Enabling the Study of Anti-Infective Efficacy and Host-Microbe Interactions. mBio **8**:e00140–17.

33. **Tal N**, **Schuldiner S**. 2009. A coordinated network of transporters with overlapping specificities provides a robust survival strategy. Proc Natl Acad Sci USA **106**:9051–9056.

34. **Ryan A**. 2017. Azoreductases in drug metabolism. Br J Pharmacol **174**:2161–2173.

35. **Akiva E**, **Copp JN**, **Tokuriki N**, **Babbitt PC**. 2017. Evolutionary and molecular foundations of multiple contemporary functions of the nitroreductase superfamily. Proc Natl Acad Sci USA **114**:E9549–E9558.

36. **Fonseca BD**, **Diering GH**, **Bidinosti MA**, **Dalal K**, **Alain T**, **Balgi AD**, **Forestieri R**, **Nodwell M**, **Rajadurai CV**, **Gunaratnam C**, **Tee AR**, **Duong F**, **Andersen RJ**, **Orlowski J**, **Numata M**, **Sonenberg N**, **Roberge M**. 2012. Structure-activity analysis of niclosamide reveals potential role for cytoplasmic pH

in control of mammalian target of rapamycin complex 1 (mTORC1) signaling. J Biol Chem **287**:17530–17545.

37. **Prosser GA**, **Copp JN**, **Syddall SP**, **Williams EM**, **Smaill JB**, **Wilson WR**, **Patterson AV**, **Ackerley DF**. 2010. Discovery and evaluation of *Escherichia coli* nitroreductases that activate the anti-cancer prodrug CB1954. Biochem Pharmacol **79**:678–687.

38. **Yadav B**, **Wennerberg K**, **Aittokallio T**, **Tang J**. 2015. Searching for Drug Synergy in Complex Dose–Response Landscapes Using an Interaction Potency Model. Comput Struct Biotechnol J **13**:504–513.

39. **Hurdle JG**, **O'Neill AJ**, **Chopra I**, **Lee RE**. 2011. Targeting bacterial membrane function: an underexploited mechanism for treating persistent infections. Nat Rev Micro **9**:62–75.

40. **van der Heijden J**, **Bosman ES**, **Reynolds LA**, **Finlay BB**. 2015. Direct measurement of oxidative and nitrosative stress dynamics in Salmonella inside macrophages. Proc Natl Acad Sci USA **112**:560–565.

41. **Lamers RP**, **Cavallari JF**, **Burrows LL**. 2013. The Efflux Inhibitor Phenylalanine-Arginine Beta-Naphthylamide (PAβN) Permeabilizes the Outer Membrane of Gram-Negative Bacteria. PLoS ONE **8**:e60666.

42. **Anes J**, **McCusker MP**, **Fanning S**, **Martins M**. 2015. The ins and outs of RND efflux pumps in *Escherichia coli*. Front Microbiol **6**:587.

43. **Zlitni S**, **Ferruccio LF**, **Brown ED**. 2013. Metabolic suppression identifies new antibacterial inhibitors under nutrient limitation. Nat Chem Biol **9**:796–804.

44. **Velkov T**, **Roberts KD**, **Thompson PE**, **Li J**. 2016. Polymyxins: a new hope in combating Gram-negative superbugs? Future Med Chem **8**:1017–1025.

45. **Delavenne EFA**, **Simon DJJ**, **Sommer MOA**, **Toft-Kehler RV**, **Aps A**. 2016. Antibacterial use of halogenated salicylanilides. WO2016038035A1

46. **Farha MA**, **Verschoor CP**, **Bowdish D**, **Brown ED**. 2013. Collapsing the proton motive force to identify synergistic combinations against *Staphylococcus aureus*. Chem Biol **20**:1168–1178.

47. **Feng X**, **Zhu W**, **Schurig-Briccio LA**, **Lindert S**, **Shoen C**, **Hitchings R**, **Li J**, **Wang Y**, **Baig N**, **Zhou T**, **Kim BK**, **Crick DC**, **Cynamon M**, **McCammon JA**, **Gennis RB**, **Oldfield E**. 2015. Antiinfectives targeting enzymes and the proton motive force. Proc Natl Acad Sci USA **112**:E7073–82.

48. **Goodwin A**, **Kersulyte D**, **Sisson G**, **Veldhuyzen van Zanten SJ**, **Berg DE**, **Hoffman PS**. 1998. Metronidazole resistance in *Helicobacter pylori* is due to null

692 mutations in a gene (rdxA) that encodes an oxygen-insensitive NADPH
693 nitroreductase. Mol Microbiol **28**:383–393.

694 49. **Baba T**, **Ara T**, **Hasegawa M**, **Takai Y**, **Okumura Y**, **Baba M**, **Datsenko KA**,
695 **Tomita M**, **Wanner BL**, **Mori H**. 2006. Construction of *Escherichia coli* K-12 in-
696 frame, single-gene knockout mutants: the Keio collection. Mol Syst Biol
697 **2**:2006.0008.

698 50. **Copp JN**, **Williams EM**, **Rich MH**, **Patterson AV**, **Smaill JB**, **Ackerley DF**.
699 2014. Toward a high-throughput screening platform for directed evolution of
700 enzymes that activate genotoxic prodrugs. Protein Eng Des Sel **27**:399–403.

701 51. **Pletzer D**, **Mansour SC**, **Hancock REW**. 2018. Synergy between conventional
702 antibiotics and anti-biofilm peptides in a murine, sub-cutaneous abscess model
703 caused by recalcitrant ESKAPE pathogens. PLoS Pathog **14**:e1007084.

704 52. **Wiegand I**, **Hilpert K**, **Hancock REW**. 2008. Agar and broth dilution methods to
705 determine the minimal inhibitory concentration (MIC) of antimicrobial substances.
706 Nat Protoc **3**:163–175.

707 53. **Copp JN**, **Mowday AM**, **Williams EM**, **Guise CP**, **Ashoorzadeh A**, **Sharrock**
708 **AV**, **Flanagan JU**, **Smaill JB**, **Patterson AV**, **Ackerley DF**. 2017. Engineering a
709 Multifunctional Nitroreductase for Improved Activation of Prodrugs and PET
710 Probes for Cancer Gene Therapy. Cell Chem Biol **24**:391–403.

711 54. **Ianevski A**, **He L**, **Aittokallio T**, **Tang J**. 2017. SynergyFinder: a web application
712 for analyzing drug combination dose-response matrix data. Bioinformatics
713 **33**:2413–2415.

714 55. **Coldham NG**, **Webber M**, **Woodward MJ**, **Piddock LJV**. 2010. A 96-well plate
715 fluorescence assay for assessment of cellular permeability and active efflux in
716 *Salmonella enterica* serovar *Typhimurium* and *Escherichia coli*. J Antimicrob
717 Chemother **65**:1655–1663.

718

719

720 **The Appendix is comprised of Tables S1-S3 and Figures S1-S6.**

721

722 **Table S1 | *E. coli* strains utilized in this study**

E. coli strain	Relevant characteristics and references [PMID]	Niclosamide MIC (μg.mL)
Wild-type BW25113	Δ*(araD-araB)567*, Δ*lacZ4787*(::rrnB-3), λ⁻, *rph-1*, Δ*(rhaD-rhaB)568*, *hsdR514* [16738554]	>32
Δ*acrA*	Deletion of AcrA membrane fusion protein of resistance-nodulation-division family	>32
Δ*acrB*	Deletion of AcrB transporter of resistance-nodulation-division family	>32
Δ*acrZ*	Deletion of AcrZ accessory protein of resistance-nodulation-division family	>32
Δ*emrA*	Deletion of EmrA membrane fusion protein of major facilitator superfamily	>32
Δ*emrB*	Deletion of EmrB transporter of major facilitator superfamily	>32
Δ*macA*	Deletion of MacA membrane fusion protein of ATP-binding cassette family	>32
Δ*macB*	Deletion of MacB transporter of ATP-binding cassette family	>32
Δ*tolC*	Deletion of TolC outer membrane factor, interacts with multiple efflux families	0.5
Δ*mdtP*	Deletion of MdtP outer membrane factor, interacts with multiple efflux families	>32
Δ7NR	Deletion of seven azo- and nitro-reductase enzymes (AzoR, MdaB, NemA, NfsA, NfsB, YcaK, YieF) from *E. coli* K-12 W3110 [4996412]	0.32
Δ7NR*tolC*	Δ7NR with additional deletion of TolC outer membrane factor	0.016

723

724 **Table S2 | Antibiotic compounds utilized in this study**

Antibiotic	Compound class	Target	BW25113 MIC[a] (μg/mL)	BW25113 ZIP score[b]	BW25113 FICI[c]	Δ*tolC* MIC[a] (μg/mL)	Δ*tolC* ZIP score[b]	Δ*tolC* FICI[c]
Chloramphenicol	Amphenicol	Protein synthesis	32	5.6	0.38	2	1.2	0.75
Tetracycline	Tetracycline	Protein synthesis	2	9.0	0.25	0.5	-0.8	0.75
Gentamicin	Aminoglycoside	Protein synthesis	0.25	-6.3	9	0.5	-8.5	8.5
Fosfomycin	Phosphonic acid	Cell wall biosynthesis	32	-0.6	1	16	-3.6	2
Cefotaxime	Cephalosporin	Cell wall biosynthesis	0.064	10.8	0.38	0.016	-4.8	3
Meropenem	Carbapenem	Cell wall biosynthesis	0.128	5.7	0.38	0.128	-5.0	2.5
Rifampicin	Ansamycin	RNA synthesis	32	1.7	1	4	-2.2	2
Metronidazole	Nitroimidazole	DNA	1024	0.4	1	1024	5.0	1.25
Nitrofurantoin	Nitrofuran	DNA/multiple	8	8.5	0.75	2	3.8	0.5
Vancomycin	Glycopeptide	Cell wall biosynthesis	256	-0.3	2	256	-4.1	1
Trimethoprim	Pyrimidine inhibitor	Folate synthesis	4	2.9	0.38	0.25	2.2	0.75
Ciprofloxacin	Quinolone	DNA synthesis	0.032	6.1	0.75	0.032	-3.0	2

725

726 [a] MIC analyses were performed in M9 minimal media

727 [b] ZIP scores were calculated from checkerboard assays with oxyclozanide in M9 minimal
728 media

729 [c] The fractional inhibitory concentration index (FICI) was calculated from checkerboard
730 assays with oxyclozanide in M9 minimal media

731

732

733

734 **Table S3 | Clinical strains utilized in this study**

Strain	Colistin MIC (µg/mL)	Relevant characteristics	Reference [PMID] or source
Pseudomonas aeruginosa			
P. aeruginosa LESB58	4	Liverpool Epidemic Strain isolate	[26814180]
P. aeruginosa NZRM4034	1	Ceftazidime/piperacillin resistant isolate	ESR resources
Acinetobacter baumannii			
A. baumannii Ab5075	0.25	Virulent wound isolate	[26991296]
A. baumannii NZRM3289	1	Urine isolate (ATCC19606)	ESR resources
Klebsiella pneumoniae			
K. pneumoniae KPLN49	0.5	Wild-type strain	[23665232]
K. pneumoniae NZRM4387	1	Extended spectrum ß-lactamase urine isolate	ESR resources
Enterobacter cloacae			
E. cloacae 218R1	0.25	Class C ß-lactamase overproducing strain	[24865555]
Escherichia coli			
E. coli E38 (serotype O78:H^-)	0.25	Human peritoneum isolate	BEI Resources
E. coli NZRM4403	0.5	ß-lactamase overproducing human blood isolate	ESR resources

735

736

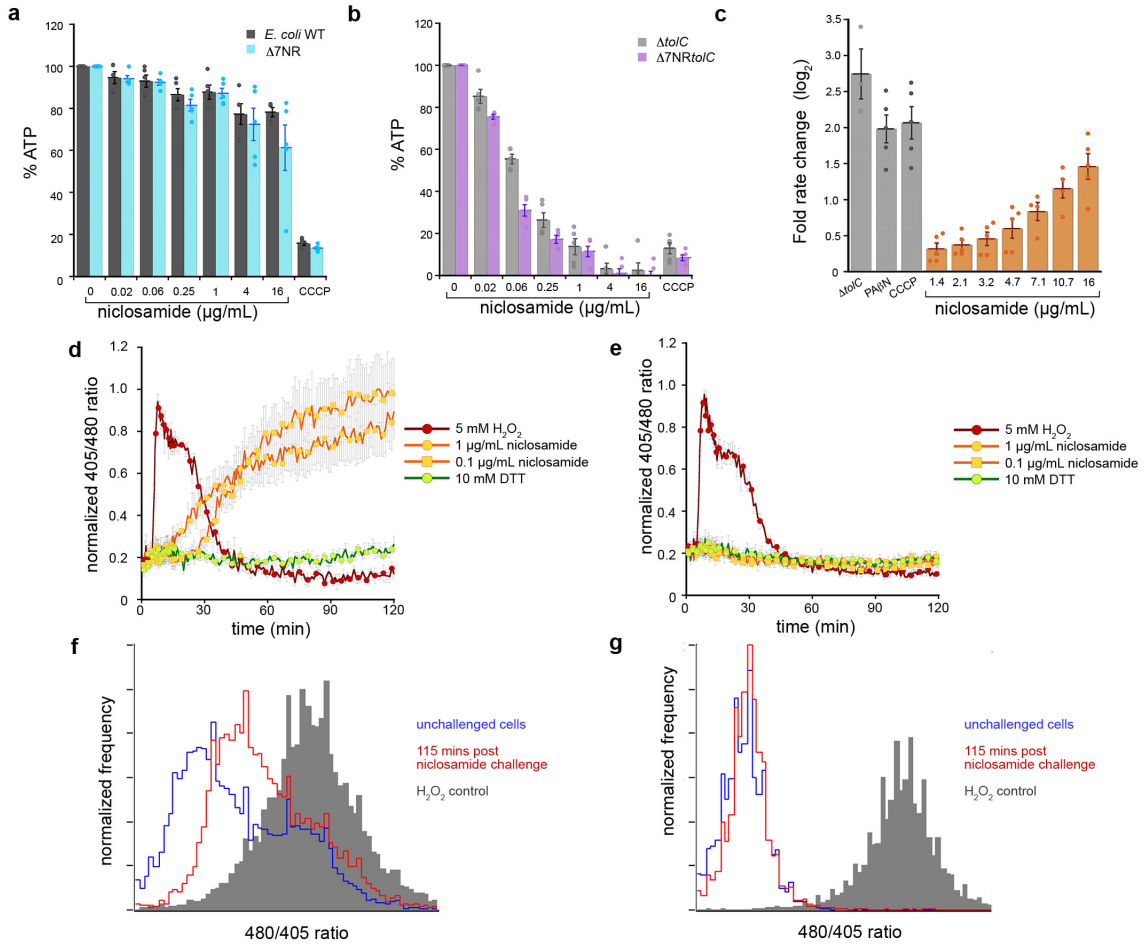

Fig S1 | Niclosamide mechanisms of action. a-b, ATP concentration was investigated using a luminescent probe, BacTiter-Glo™. Following incubation for 60 min with 0.016 - 16 μg.mL^{-1} niclosamide or 32 μg.mL^{-1} CCCP, percent ATP was determined via comparison to a DMSO control in (**a**) *E. coli* BW25113 (WT) and Δ7NR strains, and (**b**) Δ*tolC* and Δ7NR*tolC* strains. **c**, Fold rate change of Hoechst H33342 fluorescence was measured over 10 min (at 355 nm and 460 nm for excitation and emission, respectively) and compared to a DMSO-only control. Δ*tolC* was employed as a disrupted efflux control. *E. coli* cells were grown in MHB media supplemented with 5 mM EDTA for permeabilization, and were administered 28 μg.mL^{-1} PAβN, 5 μg.mL^{-1} CCCP, or 1.4 to 16 μg.mL^{-1} niclosamide. Error bars indicate SEM. **d-e**, Intracellular oxidation levels were measured over 120 min in (**d**) Δ7NR*tolC* and (**e**) Δ7NR strains constitutively expressing redox-sensitive GFP (roGFP) following administration of 5 mM H_2O_2 (oxidized control), 1 mM DTT (reduced control), 1 μg.mL^{-1} niclosamide or 0.1 μg.mL^{-1} niclosamide. **f-g**, Histograms of the 405/480-nm ratios of intracellular redox potential of (**f**) Δ7NR*tolC* and (**g**) Δ7NRcells prior to administration of niclosamide (blue) and 115 min after administration of 1 μg.mL^{-1} niclosamide. The gray histogram represents the oxidized control (10 mM H_2O_2).

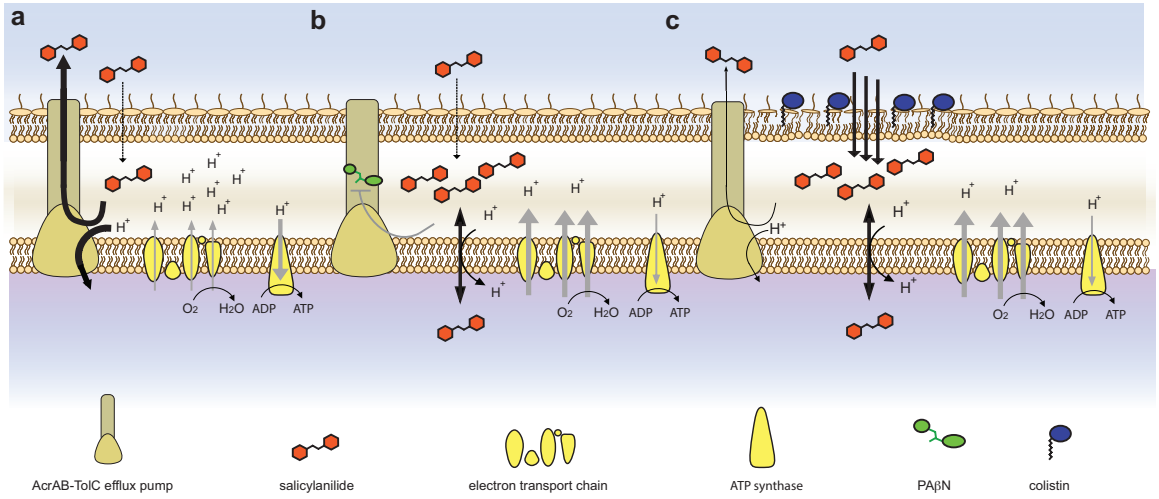

Fig S2 | Proposed salicylanilide mechanisms of action. a, A salicylanilide crosses the outer membrane but is expelled from the cell *via* TolC-mediated efflux (PMF-dependent); electron transport, membrane polarization, oxygen consumption and ATP synthesis are not affected. **b**, When TolC is inhibited by compounds such as PAβN, salicylanilides uncouple the electron transport chain, dissipate the PMF, increase oxygen consumption and decrease ATP production. **c**, When the outer membrane is disrupted via compounds such as colistin, salicylanilides rapidly enter the cell, overwhelming TolC-mediated efflux, uncoupling the electron transport chain, dissipating the PMF (inhibiting PMF-dependent efflux), increasing oxygen consumption and decreasing ATP production.

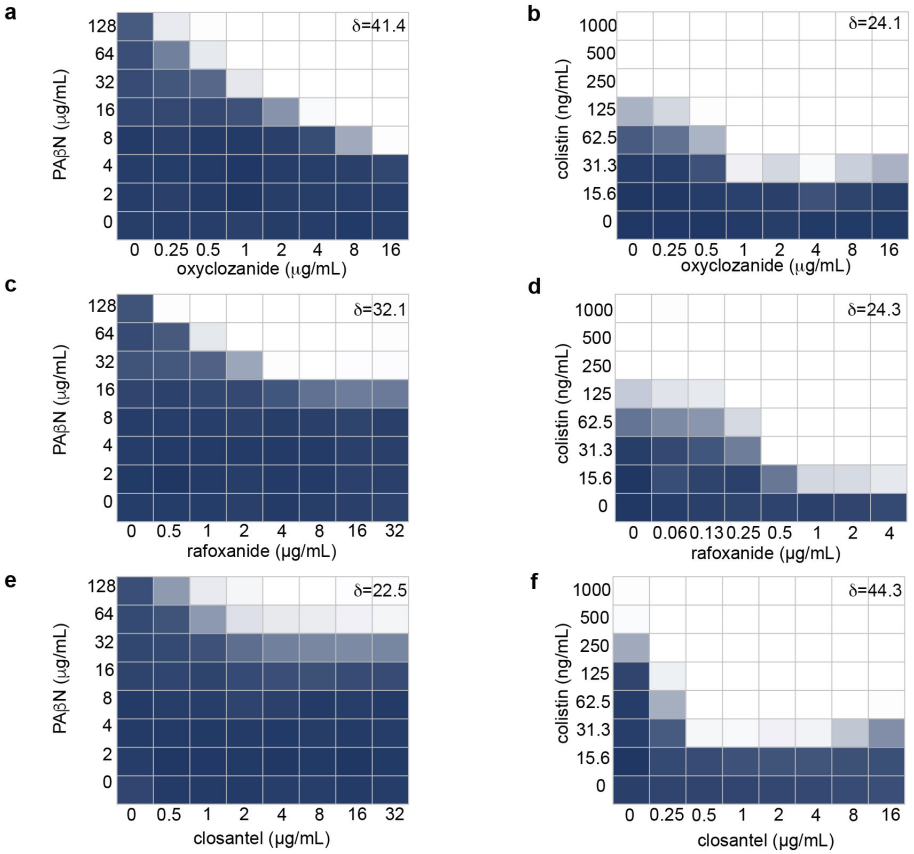

Fig. S3 | The synergistic relationships of salicylanide derivatives with PAβN and colistin. Using *E. coli* checkerboard analyses, the combined inhibitory effects of 0 to 256 μg.mL^{-1} oxyclozanide and either (**a**) 0 - 128 μg.mL^{-1} PAβN, or (**b**) 0 - 250 ng.mL^{-1} colistin; 0 - 32 μg.mL^{-1} rafoxanide and either (**c**) 0 - 128 μg.mL^{-1} PAβN, or (**d**) 0 - 250 ng.mL^{-1} colistin; and 0 - 32 μg.mL^{-1} closantel and either (**e**) 0 - 128 μg.mL^{-1} PAβN, or (**f**) 0 - 250 ng.mL^{-1} colistin were tested. Bacterial growth is shown as a heat plot. The ZIP synergy score (δ) is presented as the average interaction from the dose-response landscape. Data presented were averaged from at least 3 (typically >6) independent experiments with SEM <15%.

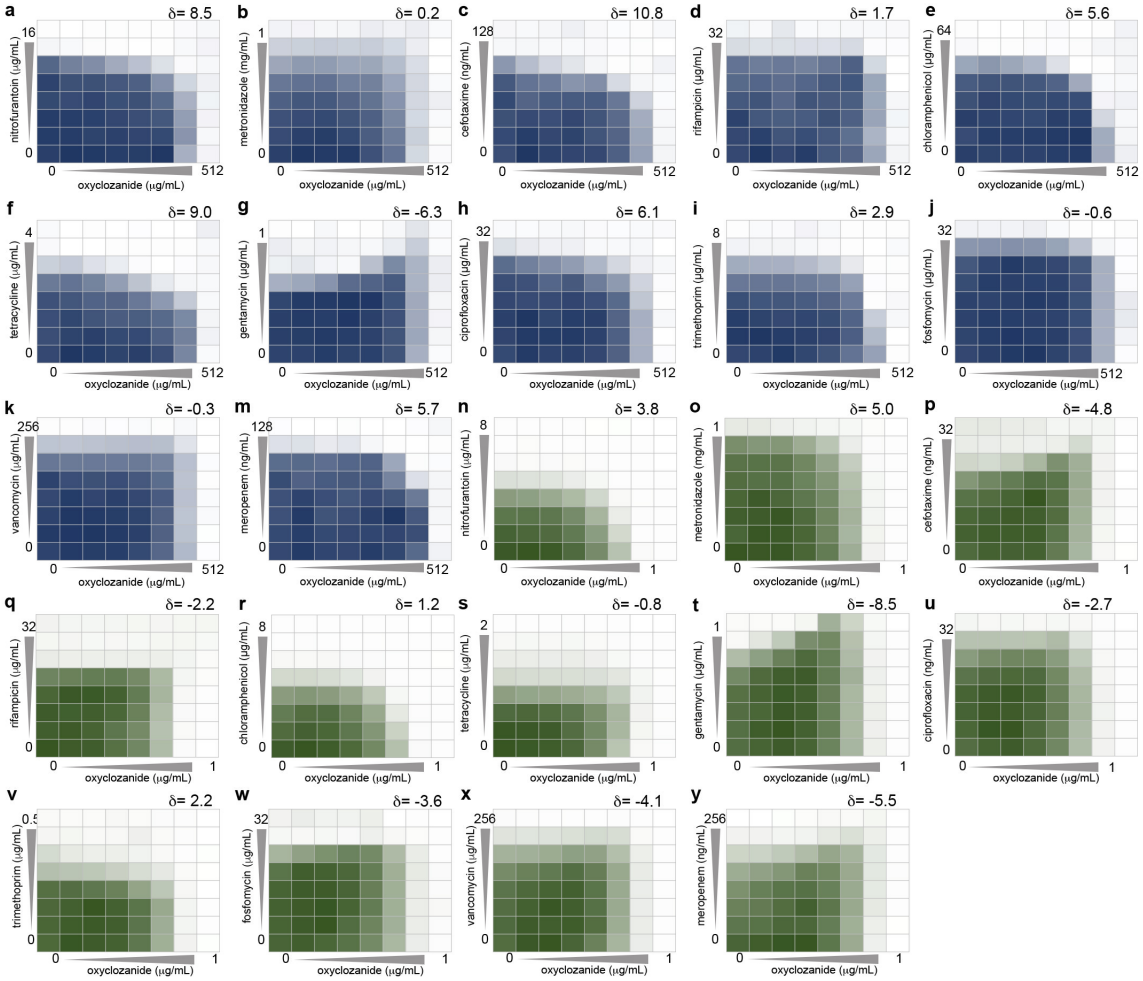

Fig. S4 | The synergistic and antagonistic relationships of oxyclozanide with diverse clinical antibiotics. a-m, The combined inhibitory effects of 0 to 512 μg.mL^{-1} oxyclozanide and either (**a**) 0 to 16 μg.mL^{-1} nitrofurantoin, or (**b**) 0 to 1 mg.mL^{-1} metronidazole, or (**c**) 0 to 128 ng.mL^{-1} cefotaxime, or (**d**) 0 to 32 μg.mL^{-1} rifampicin, or (**e**) 0 to 64 μg.mL^{-1} chloramphenicol, or (**f**) 0 to 4 μg.mL^{-1} tetracycline, or (**g**) 0 to 1 μg.mL^{-1} gentamicin, or (**h**) 0 to 32 ng.mL^{-1} ciprofloxacin, or (**i**) 0 to 8 μg.mL^{-1} trimethoprim, or (**j**) 0 to 32 μg.mL^{-1} fosfomycin, or (**k**) 0 to 256 μg.mL^{-1} vancomycin, or (**m**) 0 to 128 ng.mL^{-1} meropenem were tested against *E. coli* using checkerboard analyses in minimal media. Bacterial growth is shown as a heat plot. **n-y,** The combined inhibitory effects of 0 to 1 μg.mL^{-1} oxyclozanide and either (**n**) 0 to 8 μg.mL^{-1} nitrofurantoin, or (**o**) 0 to 1 mg.mL^{-1} metronidazole, or (**p**) 0 to 32 ng.mL^{-1} cefotaxime, or (**q**) 0 to 32 μg.mL^{-1} rifampicin, or (**r**) 0 to 8 μg.mL^{-1} chloramphenicol, or (**s**) 0 to 2 μg.mL^{-1} tetracycline, or (**t**) 0 to 1 μg.mL^{-1} gentamicin, or (**u**) 0 to 32 ng.mL^{-1} ciprofloxacin, or (**v**) 0 to 0.5 μg.mL^{-1} trimethoprim, or (**w**) 0 to 32 μg.mL^{-1} fosfomycin, or (**x**) 0 to 256 μg.mL^{-1} vancomycin, or (**y**) 0 to 256 ng.mL^{-1} meropenem were tested against *E. coli* Δ*tolC* using checkerboard analysis in minimal media. Bacterial growth is shown as a heat plot. The ZIP synergy score (δ) is presented as the average interaction from the dose-response landscape. Data presented were averaged from at least 3 (typically >6) independent experiments with SEM <15%.

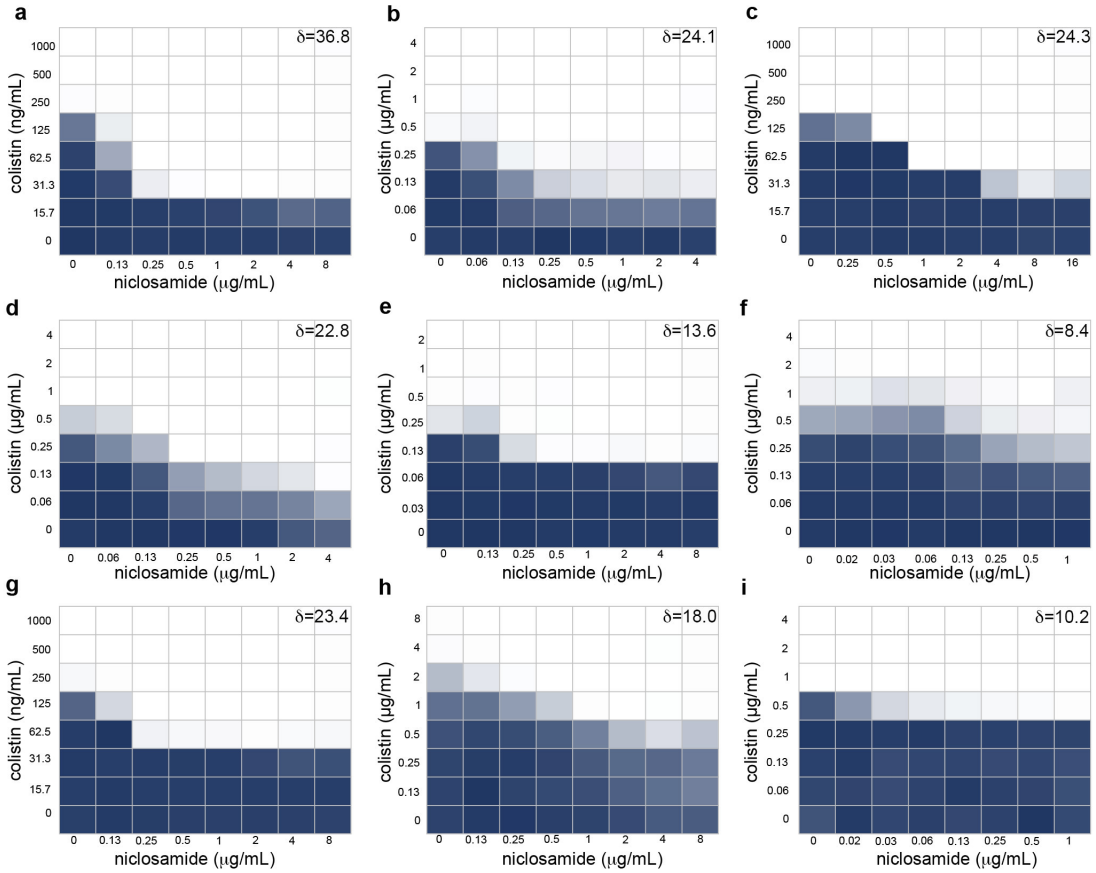

Fig. S5 | The synergistic relationships of niclosamide and colistin against clinical isolates. a-i, The combined inhibitory effects of up to 16 μg.mL^{-1} niclosamide and up to 8 μg.mL^{-1} colistin were tested using checkerboard analysis against (**a**) *E. coli* E38, or (**b**) *E. coli* NZRM4403, or (**c**) *A. baumannii* Ab5075, or (**d**) *A. baumannii* NZRM3289, or (**e**) *K. pneumoniae* KPLN649, or (**f**) *K. pneumoniae* NZRM4387 or (**g**), *E. cloacae* 218R, or (**h**) *P. aeruginosa* LESB15, or (**i**) *P. aeruginosa* NZRM4034. The ZIP synergy score (δ) is presented as the average interaction from the dose-response landscape. Data presented were averaged from at least 3 independent experiments with SEM <18%.

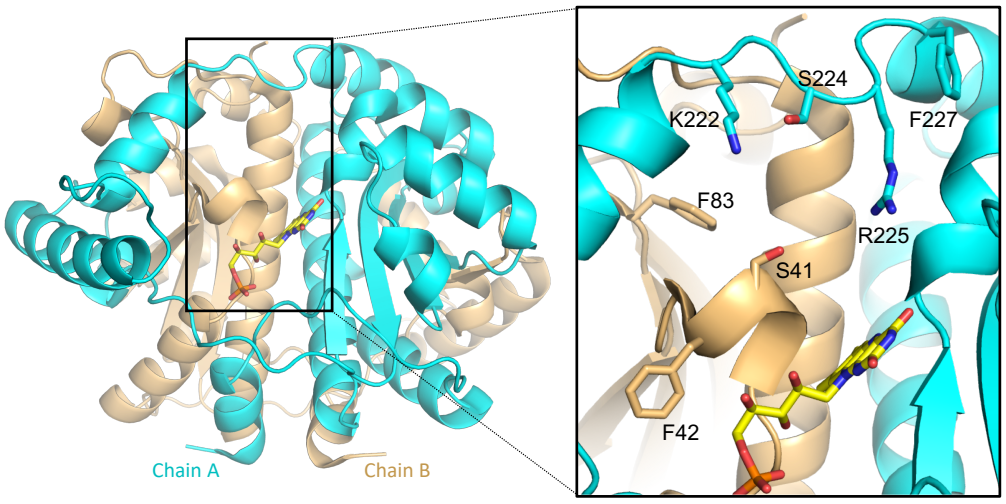

Fig. S6 | Combinatorial mutagenesis of *E. coli* NfsA. A ribbon diagram displays the dimeric structure of PBD ID: 1f5v (*E. coli* NfsA). Monomers are colored in cyan or gold respectively. FMN is depicted as a stick model with carbons colored in yellow; one active site is shown for clarity. ***Inset:*** The NfsA active site. Residues that were randomized to generate the NfsA variant library are labeled and displayed in stick models.